# Oxy-Combustion in SOFC-mGT Hybrids: Impact on $CO_2$ Capture Potential and $NO_x$ formation potential

***Maria Clara de Jesus Vieira*** [a] ***and Ward De Paepe*** [b,c]

[a] *University of Mons (UMONS), Thermal Engineering and Combustion Unit, UMONS Micro Gas Turbine Research Centre - UMARC, Mons, Belgium, mariaclara.dejesusvieira@umons.ac.be, CA*

[b] *University of Mons (UMONS), Thermal Engineering and Combustion Unit, UMONS Micro Gas Turbine Research Centre - UMARC, Mons, Belgium, ward.depaepe@umons.ac.be*

[c] *WEL Research Institute, Wavre, Belgium, ward.depaepe@umons.ac.be*

**Abstract:**
Oxy-combustion is a promising route to facilitate carbon capture in gas turbine and hybrid power systems by enhancing the concentration of $CO_2$ in the flue gases and thereby simplifying downstream separation. In solid oxide fuel cell–micro gas turbine (SOFC–mGT) hybrid cycles, oxy-combustion can be exploited not only to provide $CO_2$-rich exhaust streams that are more compatible with capture processes, but also to significantly reduce $NO_x$ formation through the removal of atmospheric nitrogen from the oxidant stream. However, a systematic assessment of how oxy-combustion conditions and fuel utilization factor jointly affect $CO_2$ enrichment, $NO_x$ formation potential, and overall cycle performance in SOFC–mGT hybrids is still lacking.
In this work, an SOFC–mGT hybrid cycle is modeled in Aspen Plus to investigate the impact of oxy-combustion on flue gas composition and emissions, focusing on $CO_2$ and $NO_x$ reduction potential. The specific aim of this study is to quantify the combined influence of fuel utilization factor and the oxidant composition on the feasibility of integrating oxy-combustion into SOFC–mGT systems, thereby identifying operating regimes that balance $CO_2$ capture readiness, $NO_x$ mitigation, and cycle efficiency. Results show that partial oxy-combustion, moderate $O_2$ enrichment ($x_{\mathrm{O_2,ox}} \approx 0.4$–$0.6$) combined with high fuel utilization ($U_f \geq 0.5$), simultaneously achieves $CO_2$ concentrations above 22 %, suppresses $NO_x$ formation potential by eliminating $N_2$ from the oxidant, and maintains turbine temperatures within feasible bounds, making it a practically attractive strategy for carbon capture integration in hybrid power systems.

**Keywords:**
SOFC-mGT hybrid; oxy-combustion; $CO_2$ capture; $NO_x$ formation potential; fuel utilization.

# 1. Introduction

Solid oxide fuel cell–micro gas turbine (SOFC–mGT) hybrid cycles have been investigated for decades as high-efficiency power systems that combine electrochemical conversion in the fuel cell with turbomachinery-based recovery of remaining chemical and sensible enthalpy in the exhaust [1–4]. Beyond their potential for high net electrical efficiency, hybrid cycles offer additional degrees of freedom for thermal management and power split, but also introduce strong coupling between electrochemical operating conditions, post-anode oxidation, and turbomachinery temperature limits [4,5]. At the same time, decarbonization constraints and waste-gas utilization motivate renewed interest in converting carbon-containing low-calorific fuels (e.g., $CO_2$-diluted natural gas and flare gases) into electricity with improved efficiency compared to standalone micro gas turbines [6–8]. However, flare-gas-to-power remains underexploited in practice, and fuel variability (light hydrocarbons, $CO_2$, and inerts) complicates both cycle integration and emissions control [6, 9].
Most SOFC–GT capture concepts rely on post-combustion separation for $CO_2$ recovery, but small-scale systems face strong penalties when treating nitrogen-diluted exhaust streams [10]. Oxy-

combustion and oxygen-enriched combustion are therefore attractive because reducing the $N_2$ content of the oxidant increases the $CO_2$ concentration in the flue gas and can simplify downstream separation compared to conventional air firing [11]. From an emissions standpoint, removing atmospheric nitrogen also suppresses the dominant reactant pool for thermal NO formation, which is commonly described using extended Zeldovich chemistry and is dependent on high-temperature residence time [12, 13].

In SOFC–mGT hybrids, the combustor is typically fed by SOFC anode off-gas rather than a fresh, well-characterized fuel stream; consequently, combustor inlet composition depends on fuel utilization and fuel composition, and the combustor simultaneously acts as a constraint-enforcing component for turbine inlet temperature [5, 8]. This effect is especially important under oxygen-enriched conditions. In this case, the higher $O_2$ concentration can increase the flame temperature and promote thermal $NO_x$ formation as long as $N_2$ remains present. Therefore, intermediate oxidizer compositions between air-fired and nitrogen-free operation may create a $NO_x$ "risk window" [12, 13]. As a result, a systematic evaluation of oxidant composition, fuel utilization, and fuel composition is needed to identify operating regions where $CO_2$ enrichment yields capture-ready exhaust streams without unacceptable penalties in operability and performance, and without elevated $NO_x$ formation in intermediate enrichment regimes.

In our recent work, we developed a steady-state Aspen Plus model of an externally reformed SOFC–mGT hybrid using Elcogen SOFC stacks [14] coupled to the 10 kWe MITIS Micro-10 micro gas turbine [15], and demonstrated the influence of fuel utilization and dry-reformed $CH_4/CO_2$ flare-gas surrogates on cycle efficiency, turbomachinery temperatures, and anode-off-gas composition [16]. The present paper adopts the same baseline configuration and modelling framework [16] but shifts the focus to the oxy-combustion dimension itself: instead of air firing, the SOFC fuel utilization and oxidant composition are systematically varied from air to oxygen-rich and nitrogen-free limits to quantify (i) $CO_2$ enrichment and capture-relevant exhaust indicators, (ii) thermal-$NO_x$ formation potential across the enrichment-to-oxy transition, and (iii) the associated trade-offs in cycle performance and turbine temperature feasibility.

A key modelling challenge is that system-level parametric sweeps require robust and repeatable combustion calculations across large composition ranges, while thermal NO formation is inherently kinetic rather than equilibrium-controlled. Accordingly, the cycle simulations are used to provide consistent thermochemical states and exhaust compositions, while $NO_x$ is evaluated as a formation potential through kinetic post-processing with a residence-time sweep using detailed gas-phase chemistry [12, 17, 18]. This work aims to establish a framework for identifying operating windows in SOFC–mGT hybrids where oxy-combustion enhances $CO_2$ capture readiness and mitigates nitrogen-driven $NO_x$ formation, while maintaining turbine temperature limits and minimizing efficiency losses.

# 2. System description

This section presents the modeled SOFC–mGT hybrid cycle, including its overall concept, process boundaries, and key component specifications. The process layout is first outlined, followed by details on the oxidant stream transitioning from air-fired to oxygen-rich conditions for oxy-combustion.

## 2.1. System concept and boundaries

The system considered, shown in Fig 1, is an atmospheric SOFC–mGT hybrid cycle in which the SOFC delivers electrical power and a hot anode off-gas stream that is subsequently oxidized in a dedicated combustor to provide the thermal input of the micro gas turbine. The present work adopts the same baseline configuration and component philosophy as our recent SOFC–mGT study [16], but focuses on the impact of oxidant composition (air to oxygen-rich to nitrogen-free limits) and SOFC fuel utilization on flue-gas composition, capture readiness, and thermal-$NO_x$ formation potential.

The analysis is performed at steady state conditions. The system boundary includes the SOFC stack, the post-anode combustor, the turbomachinery (turbine, compressor, shaft/generator), and the main

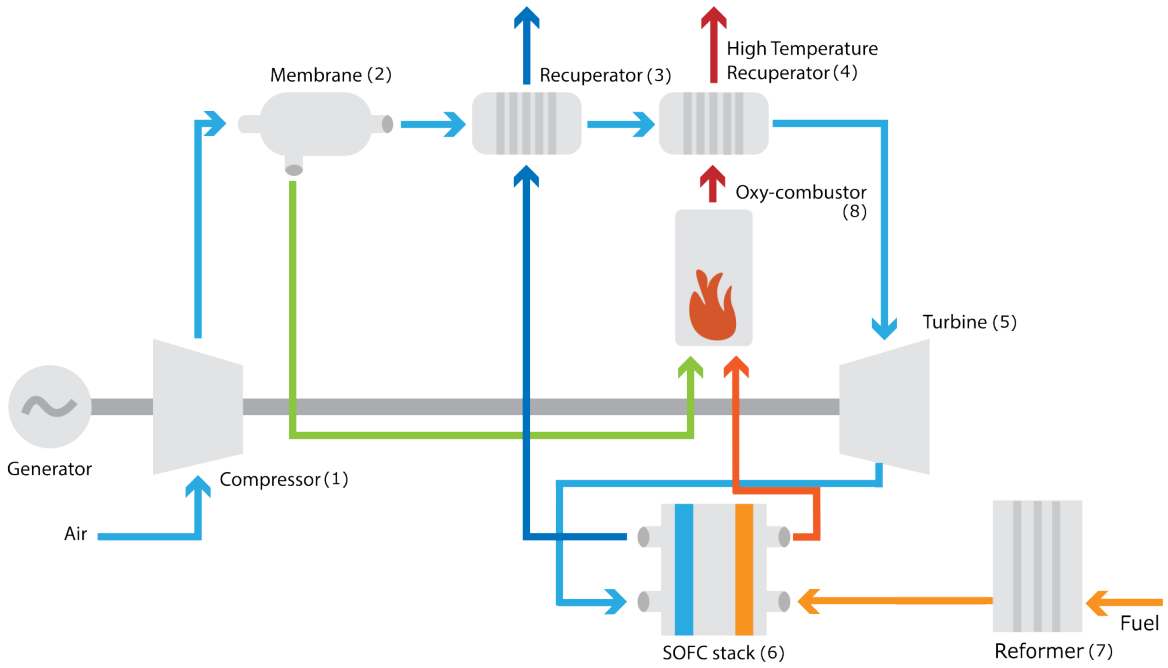


**Figure 1**: Considered SOFC–mGT hybrid cycle, including the compressor (1), membrane (2), recuperator (3), high temperature recuperator (4), turbine (5), SOFC stack (6), reformer (7) and the oxy-combustor (8).

heat-exchange devices used to achieve the required thermal integration between the SOFC and the mGT. When oxygen-enriched or oxy-fired operation is considered, the oxygen supply is treated as part of the overall system boundary through an equivalent oxidant stream specification. Unless explicitly stated otherwise, auxiliary subsystems not essential to establish the thermodynamic state of the working fluid (e.g., detailed balance-of-plant controls, start-up hardware) are not modeled.

## 2.2. Process layout

Fig 1 summarizes the cycle layout. Ambient air enters the compressor (1), is pressurized, and is then routed through the recuperative heat-exchange network (3 and 4) to reach the turbine (5) and, from there, the SOFC cathode (6) inlet temperature required for stable stack operation. In oxy-fired cases, an air separation unit (ASU) or oxygen membrane (2) provides the required $O_2$-rich oxidant stream (detailed in Section 2.3.). The heated oxidant stream then flows through the SOFC cathode channels (6), where oxygen is consumed electrochemically in proportion to the imposed fuel utilization. The hot cathode exhaust provides heat for recuperation (3) before leaving the system.

On the fuel side, a single flare-gas surrogate fuel (50% $CH_4$ + 50% $CO_2$) is considered throughout this work to isolate the effects of oxidant composition and fuel utilization $U_f$ on cycle behaviour and exhaust properties [16]. The fuel cell stack (6) is operated at prescribed $U_f$ over the range $U_f \in [0.3, 0.8]$, which determines the fraction of electrochemically active fuel converted in the cell and therefore sets the residual chemical energy and composition of the anode off-gas. For each $U_f$, the resulting anode off-gas provides the combustor (8) inlet fuel stream and is sent to a dedicated post-anode combustor (8), where any remaining combustible species are oxidized. This dedicated anode-off-gas oxidation stage (i.e., separated from cathode exhaust mixing upstream) is retained to enable $CO_2$-rich exhaust streams under oxygen-enriched and oxy-fired conditions. This coupling ensures that changes in $U_f$ propagate to combustor heat release, turbine inlet temperature (TIT), and exhaust composition, allowing operating regions to be identified based on capture readiness, temperature feasibility, and $NO_x$ formation potential.

The compressed heated air stream is expanded in the turbine (5) to produce shaft work, which drives the compressor (1) and an electrical generator. The turbine exhaust provides the hot-side thermal source for the SOFC cathode (6) before going for the recuperator for heat exchange (3). The flue-gas

composition, in particular dry $CO_2$, $H_2O$, and residual $O_2$, is used to evaluate $CO_2$ capture readiness and its sensitivity to oxidant composition and $U_f$.

### 2.3. Oxidant specification: air to oxygen-rich to nitrogen-free

To study the transition from conventional air firing to oxygen-rich and nitrogen-free operation, the oxidant composition supplied to the post-anode combustor is parametrically varied from air to an $O_2$-rich mixture and finally to the nitrogen-free limit. Oxygen enrichment is modeled using high-selectivity polymeric or ceramic oxygen transport membranes, which currently achieve 40–42% of $O_2$ purity; the analysis extrapolates beyond this to establish technology targets for full oxy-combustion. In the "air-fired" reference cases, the oxidant is atmospheric air. In the oxygen-enriched cases, the $O_2$ mole fraction is increased while the balance is primarily $N_2$. In the nitrogen-free cases, the oxidant is specified as $O_2$ without $N_2$, representing the oxy-fired limit. This approach enables a systematic assessment of how reducing $N_2$ dilution changes (i) $CO_2$ enrichment in the exhaust and (ii) thermal-$NO_x$ formation potential across the enrichment-to-oxy transition.

## 3. Methodology

This section describes the steady-state modeling framework used to evaluate oxy-combustion effects in the SOFC–mGT hybrid cycle. The approach builds on our baseline model by implementing a parametric sweep of SOFC fuel utilization ($U_f$) and post-combustion oxidant composition ($x_{\mathrm{O_2,ox}}$), complemented by kinetic post-processing for thermal-$NO_x$ formation potential.

### 3.1. Base SOFC–mGT model

The present work uses a steady-state Aspen Plus model of an atmospheric SOFC–mGT hybrid cycle adopting the same baseline configuration as our recent study [16] and the same underlying modelling framework. The goal is not to re-establish the baseline model, but to extend it toward a systematic oxidant-composition sweep (air $\rightarrow$ oxygen-enriched $\rightarrow$ nitrogen-free) and to quantify its consequences for flue-gas composition, capture readiness, thermal-$NO_x$ formation potential, and cycle performance.

Unless otherwise stated, the parametric space is defined by $U_f \in [0.3,\ 0.8]$ and by an oxidant sweep spanning $x_{\mathrm{O_2,ox}} \in [0.21,\ 1.0]$, where $x_{\mathrm{O_2,ox}}$ denotes the $O_2$ mole fraction of the oxidant stream supplied to the post-anode combustor. The SOFC is operated at atmospheric pressure with a quasi-isothermal stack temperature assumption, and fuel utilization is imposed as a control variable. For each operating point, the prescribed fuel utilization factor $U_f$ determines the fraction of electrochemically active fuel converted in the cell and therefore sets the residual chemical energy and composition of the anode off-gas entering the post-anode combustor.

The micro gas turbine subsystem is represented as an externally fired recuperated cycle; the compressor, turbine, and heat exchangers (including the high-temperature recuperator providing thermal coupling to the SOFC exhaust) are modeled in Aspen Plus to provide consistent steady-state mass and energy balances across the full parametric sweep, while turbine inlet and outlet temperatures (TIT and TOT) are tracked as primary operability indicators.

For each case, the net electrical efficiency is computed on a lower heating value (LHV) basis as:

$$\eta_{\mathrm{el,net}} = \frac{\dot{W}_{\mathrm{el,net}}}{\dot{m}_{\mathrm{f}}\,\mathrm{LHV}}, \tag{1}$$

where $\dot{W}_{\mathrm{el,net}}$ is the net electrical power output of the hybrid system (SOFC AC power plus turbomachinery shaft power converted to electricity, minus auxiliary loads included in the cycle model). Because the present paper focuses on the intrinsic influence of oxidant composition and SOFC fuel utilization, an explicit oxygen-production penalty is not included.

A single fuel surrogate is deliberately retained throughout this study to isolate the thermochemical effects of oxidant composition and $U_f$ from fuel-composition variability; sensitivity to fuel composition

is reserved for a dedicated follow-up investigation.

## 3.2. Oxy-combustion implementation

The oxidant sweep is defined by the $O_2$ mole fraction in the oxidant stream, $x_{\mathrm{O_2,ox}}$. In the oxygen-enriched cases, the balance of the oxidant stream is primarily $N_2$; in the nitrogen-free cases, $N_2$ is removed entirely and the oxidant is specified as pure $O_2$. For each point in the sweep and each selected $U_f$, the full cycle is re-solved to ensure self-consistent combustor inlet conditions and turbomachinery states.

The post-anode combustor is modeled as an adiabatic equilibrium reactor using the Aspen Plus `RGibbs` block. In Aspen, `RGibbs` performs equilibrium calculations by minimizing the total Gibbs free energy of the mixture subject to elemental balance constraints, which provides a robust solution strategy over wide composition ranges [19]. This representation is therefore suited for system-level sweeps aimed at assessing exhaust $CO_2$ enrichment, oxygen slip, and turbine-temperature feasibility as functions of oxidant composition and $U_f$, but it does not represent finite-rate pollutant chemistry; consequently, $NO_x$ is evaluated via kinetic post-processing (Section 3.3.).

$CO_2$ capture readiness is evaluated primarily through the dry $CO_2$ mole fraction in the flue gas, together with supporting indicators such as residual $O_2$ (oxygen slip). In addition to composition, the associated changes in combustor adiabatic temperature and the resulting TIT/TOT are tracked to identify feasibility limits and to determine whether oxygen-enriched or nitrogen-free operation remains compatible with the targeted turbomachinery operating envelope.

Oxygen-enriched and nitrogen-free oxidant streams are imposed at the combustor inlet using a simplified separator (`SEP`) representation that enforces the target $x_{\mathrm{O_2,ox}}$ without accounting for separation power, oxygen compression, or purity-dependent losses. This simplification isolates the thermochemical and cycle-integration effects of oxidant composition from the technology-dependent oxygen production penalty.

## 3.3. $NO_x$ evaluation (formation potential)

Thermal $NO_x$ formation is governed by highly temperature-dependent kinetics and depends strongly on high temperature residence time; therefore, $NO_x$ is evaluated here as a *formation potential* using kinetic post-processing rather than being taken from equilibrium cycle calculations.

For each case (specified by $U_f$ and $x_{\mathrm{O_2,ox}}$), the combustor inlet thermochemical state is extracted from the steady-state cycle simulation: inlet temperature $T_{\mathrm{comb,in}}$, pressure $p_{\mathrm{comb,in}}$, and composition vector $\boldsymbol{X}_{\mathrm{comb,in}}$ (mole fractions). The inlet state is formed by mixing the SOFC anode off-gas stream with the oxidant stream specified for the considered enrichment level; molar flow rates from the cycle solution are retained so that the equivalence ratio and dilution level implied by the integrated system are preserved in the kinetics post-processing.

$NO_x$ is computed using a zero-dimensional, well-mixed reactor model intended to represent an idealized combustor control volume. The reactor is treated as adiabatic at constant pressure ($p = p_{\mathrm{comb,in}}$), and a residence-time sweep is performed to bound the sensitivity of NO formation to uncertain combustor time scales. Accordingly, each operating point is associated with a band of $NO_x$ values rather than a single deterministic number, and the residence-time range is reported together with the results.

Gas-phase kinetics are represented using GRI-Mech 3.0, which is a natural-gas combustion mechanism optimized against targets that include prompt-NO formation and includes 53 species and 325 reactions [17]. Time integration is carried out using reactor network methods, as implemented in Cantera [18].

$NO_x$ is reported as NO + $NO_2$ on a dry basis, using

$$\mathrm{NO}_x\ (\mathrm{ppm_{vd}}) = 10^6\,\frac{x_{\mathrm{NO}} + x_{\mathrm{NO_2}}}{1 - x_{\mathrm{H_2O}}}. \tag{2}$$

When comparison to standard reporting conventions is required, $NO_x$ may additionally be referenced

to a fixed oxygen content; because oxygen slip can vary substantially across the oxidant sweep, such normalized values are reported alongside the raw dry-basis value.
Across the air-to-oxy transition, it is expected that two competing effects are captured: increasing oxygen enrichment can raise adiabatic temperature while $N_2$ remains present (potentially increasing thermal NO formation rates), whereas approaching nitrogen-free oxidant removes the dominant nitrogen reactant pool and drives thermal $NO_x$ toward negligible values under the present assumptions. The computed values are therefore interpreted as formation potential and used to locate enrichment ranges that may elevate $NO_x$ and to identify operating windows where $CO_2$ enrichment and low $NO_x$ are simultaneously achieved.

# 4. Results

This section presents contour maps of performance indicators across the $U_f \in [0.3, 0.8]$ and $O_2$ fraction $x_{O_2,\mathrm{ox}} \in [0.21, 1.0]$ ranges. The analysis quantifies $CO_2$ enrichment potential (section 4.1.), thermal-$NO_x$ formation risk (section 4.2.), turbine thermal limits (TIT/TOT), and efficiency trade-offs (section 4.3.), culminating in optimal operating windows that balance capture readiness with cycle performance.

## 4.1. $CO_2$ enrichment and capture readiness

The two operating parameters span the ranges $U_f \in [0.3, 0.8]$ and $x_{O_2} \in [0.21, 1.0]$, with the resulting dry $CO_2$ content varying between approximately 11% and 36% (Fig 2). The $CO_2$ concentration is reported on a dry basis, i.e., after virtual removal of water vapor from the flue gas, as this convention eliminates the variability introduced by moisture content, and provides a directly comparable metric across different system configurations and relevant to downstream capture processes, where water is typically condensed out prior to the separation unit [20]. The dry flue gas (after $H_2O$ removal) consists primarily of $CO_2$, $O_2$, $N_2$, with traces of CO, $H_2$, $CH_4$ from incomplete combustion/fuel slip. $N_2$ dominates at low $x_{O_2,\mathrm{ox}}$ (air-fired: ∼70–75%), dropping to zero at $x_{O_2,\mathrm{ox}} = 1.0$.

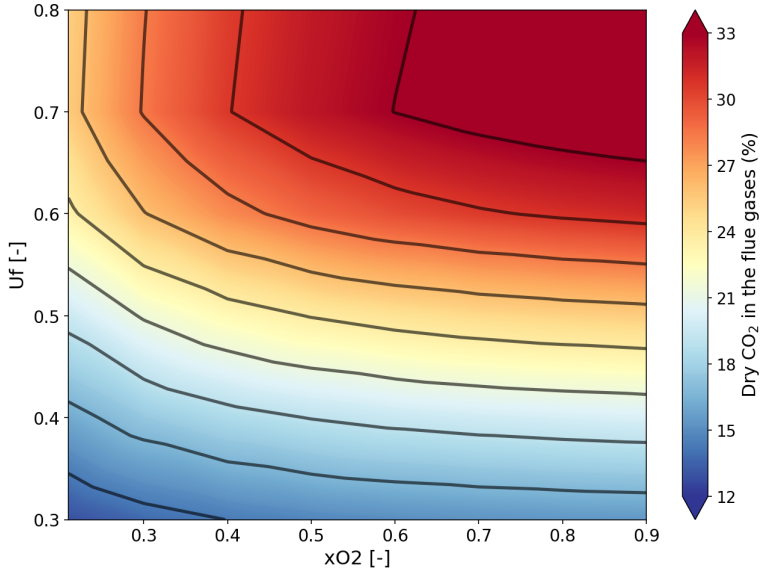


**Figure 2**: Dry $CO_2$ mole fraction in the flue gas as a function of SOFC fuel utilization $U_f$ and oxidant $O_2$ fraction $x_{O_2,\mathrm{ox}}$. $CO_2$ fraction increases monotonically with both $U_f$ and $x_{O_2,\mathrm{ox}}$, reaching values above 30 % at high $U_f$ and $x_{O_2,\mathrm{ox}}$.

Post-combustion $CO_2$ capture technologies become significantly more cost-effective and energetically favorable as the feed $CO_2$ concentration increases [21]. At concentrations typical of air-fired systems (around 15–20 vol%), MEA-based absorption already achieves specific reboiler duties of 3.6–3.8 MJ $kg^{-1}$ $CO_2$ [22]; below this threshold, the separation penalty rises steeply. Conventional SOFC operation with air ($x_{O_2} \approx 0.21$) and moderate fuel utilization ($U_f \approx 0.5$–$0.6$) yields dry $CO_2$

concentrations in the range of 14–18% as evidenced by the lower-left region of the map.
The figure identifies the path toward maximum $CO_2$ enrichment: both $U_f$ and $x_{O_2}$ must be pushed toward their upper bounds simultaneously. Operating at $U_f \to 0.8$ ensures that the largest possible fraction of the carbon-bearing fuel is electrochemically oxidized within the stack, directly maximizing $CO_2$ production at the anode outlet [23]. Simultaneously, increasing $x_{O_2}$ toward unity eliminates nitrogen as a diluent in the cathode stream, preventing its introduction into the recirculated or mixed exhaust (an effect analogous to the nitrogen suppression strategy employed in oxy-fuel combustion [8]). The combined effect in the upper-right corner of the map yields dry $CO_2$ fractions exceeding 32%, a level at which even more energy-efficient capture routes such as low-temperature condensation or physical absorption become accessible [23].
The iso-concentration contours define operating envelopes within which a given capture technology remains viable. For example, a capture system requiring a minimum dry $CO_2$ feed of 20%, as is typical for vacuum pressure swing adsorption (VPSA)-based processes [24], can be satisfied across a broad range of ($x_{O_2}$, $U_f$) combinations in the upper half of the map, providing operational flexibility. Notably, even moderate oxygen enrichment ($x_{O_2} \approx 0.5$–$0.6$) combined with high fuel utilization ($U_f \geq 0.7$) already achieves concentrations above 25%, suggesting that a partial air separation unit at the cathode inlet could offer an attractive trade-off between enrichment cost and capture performance without requiring a full oxy-fuel configuration [8, 25].

## 4.2. $NO_x$ formation potential under enrichment-to-oxy transition

The $NO_x$ formation potential exhibits a non-monotonic trend with respect to oxygen enrichment, as shown in Fig 3. Starting from the air-fired baseline, $NO_x$ progressively decreases with $x_{O_2}$ until reaching a low region at very high $x_{O_2}$ concentrations. In this regime, increasing the oxidizer oxygen fraction raises the adiabatic flame temperature but concurrently reduces the nitrogen concentration available for the extended Zeldovich reactions. As a result, despite the higher thermal conditions, the overall $NO_x$ formation rate decreases due to the diminished $N_2$ participation in the reaction chain.

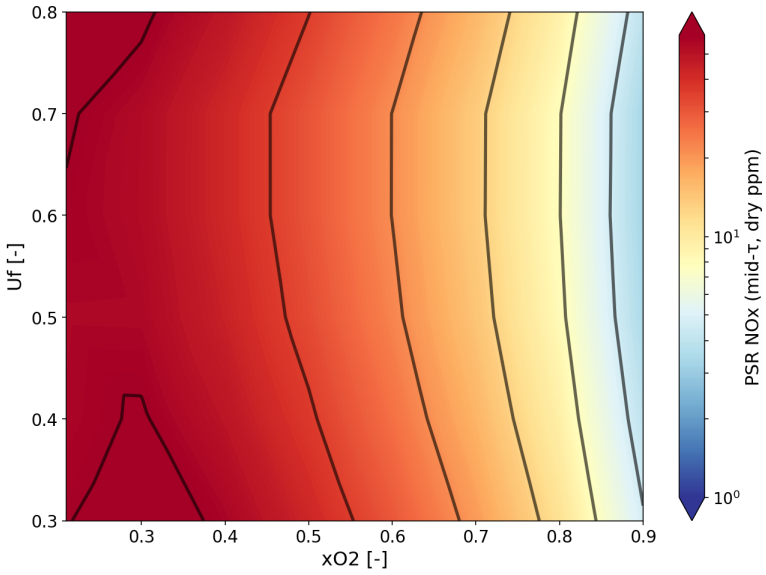


**Figure 3**: Thermal-$NO_x$ formation potential (zero-dimensional well-stirred reactor, mid-residence-time, dry ppm) versus $U_f$ and $x_{O_2,ox}$, obtained by kinetic post-processing with GRI-Mech 3.0. A "risk window" of elevated $NO_x$ (>10 ppm) appears at intermediate/low enrichment ($x_{O_2,ox} \approx 0.21$–$0.7$), driven by higher adiabatic temperatures while higher concentrations of $N_2$ are still present.

At intermediate $U_f$ values (0.5–0.7), the effective fuel slip on the anode side decreases enough to limit the local heat release, resulting in moderate flame temperatures. This thermal moderation suppresses the extended Zeldovich mechanism, leading to lower $NO_x$ concentrations even at constant oxidizer composition.

Beyond $x_{O_2,ox} > 0.7$, a sharp decline in $NO_x$ concentration is observed, converging toward negligible values under almost fully oxy-combustion conditions. Here, the absence of $N_2$ in the oxidizer effectively suppresses thermal-$NO_x$ formation despite the persistence of elevated flame temperatures. The remaining minor formation potential likely originates from prompt or residual-Fuel-N mechanisms, both limited by the reduced presence of hydrocarbon radicals and nitrogen-bearing intermediates.

## 4.3. Net trade-offs and operating windows

TIT increases strongly (from 630°C to 930°C) with decreasing $U_f$ across the full $x_{O_2,ox}$ range, driven by reduced heat-capacity dilution of the combustor products as more fuel slips from the SOFC anode exhaust (Fig 4). The substitution of $N_2$ with $CO_2$/$H_2O$ amplifies this TIT rise per unit heat release, with $O_2$-enrichment showing a non-monotonic effect: moderate gains up to $x_{O_2,ox} \approx 0.5$ followed by decline at higher fractions due to reduced thermal dilution.

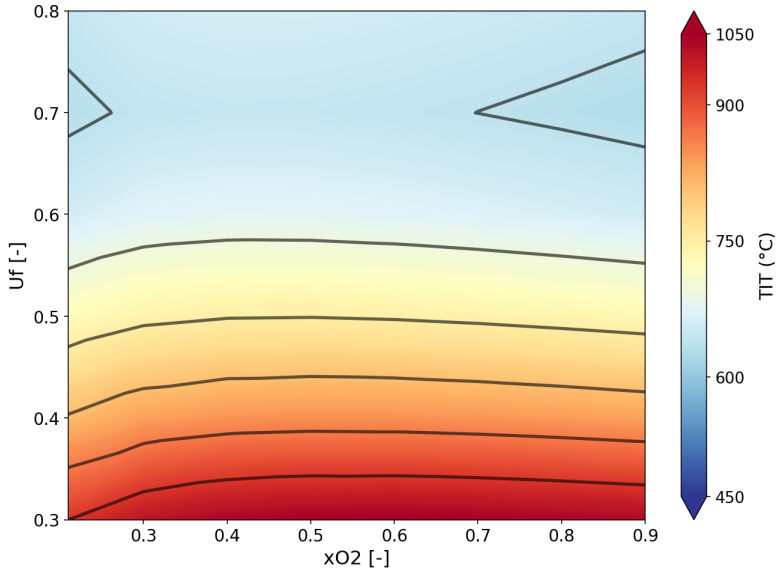


**Figure 4**: Turbine inlet temperature (TIT, °C) as a function of $U_f$ and $x_{O_2,ox}$. TIT rises sharply with the decrease of $U_f$ due to reduced $N_2$ heat-capacity dilution; low $U_f$ exacerbates this by increasing fuel slip and heat release in the combustor.

At the air-fired baseline ($x_{O_2,ox} = 0.21$), the combustion process remains markedly dilute, resulting in TIT values lower than with increased $x_{O_2,ox}$ fractions. These low temperatures are characteristic of the SOFC anode off-gas combustion, where large amounts of inert $N_2$ and residual steam absorb a significant fraction of the released heat. As $U_f$ increases toward 0.6–0.7, the available fuel for post-anode combustion decreases sharply, lowering the heat release and driving TIT down to approximately 580°C. Conversely, at low $U_f$ ($\approx$ 0.3–0.4), higher fuel slip from the SOFC anode leads to more exothermic combustion, elevating TIT toward the turbine material limit (1000°C) but remaining safely below this physical constraint.

The sensitivity of TIT to oxygen fraction highlights a small interdependence between combustor stoichiometry and system-level thermal constraints. For intermediate $x_{O_2,ox}$ values (0.4–0.7), TIT remains constant. Beyond this regime ($x_{O_2,ox} > 0.7$), TIT starts to decrease for all $U_f$ values. For intermediate $x_{O_2,ox}$ values (0.21–0.3), TIT decreases for the same $U_f$ value.

Turbine outlet temperature (TOT) follows the same qualitative trends as TIT but at lower absolute levels due to energy extraction across the turbine stages (Fig 5). In general, TOT remains below 750 °C, providing an appropriate margin for downstream recuperation. The red contour marks the minimum temperature (580 °C) required to the SOFC cathode preheating. Regions where TOT falls below this limit correspond primarily to high/intermediate $U_f$ ($> 0.5$), where limited anode slip combined with reduced mass flow leads to incomplete energy utilization and lower post-expansion gas temperatures.

Conversely, the high-$U_f$ regime defines a thermally balanced operating window achieving both TIT $<$

1000 °C and TOT $>$ 580 °C. Within this domain, adequate heat release supports efficient recuperation without approaching turbine material limits, offering a pathway for stable oxy-combustion integration with SOFC–microturbine systems.

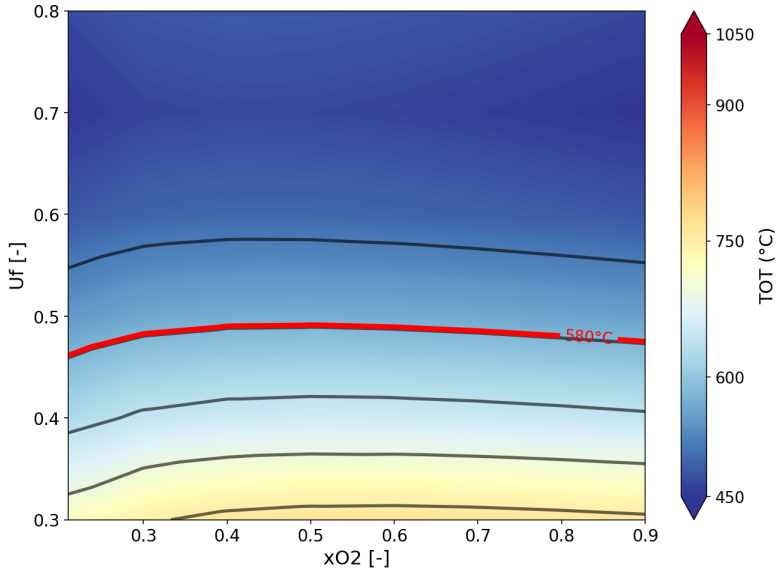


**Figure 5**: Turbine outlet temperature (TOT, °C) versus $U_f$ and $x_{\mathrm{O_2,ox}}$. TOT follows TIT trends but is moderated by turbine expansion; the red contour marks the TOT limit of 580 °C required for the SOFC cathode inlet temperature.

Collectively, these temperature maps confirm that oxygen enrichment increases combustor product temperatures by diminishing inert dilution and increasing the effective enthalpy of combustion. The identified operating window coincides with the high-$CO_2$, low-$NO_x$ regions in Figs 2 and 3, underscoring that thermochemical feasibility and formation potential mitigation can be jointly achieved through appropriate selection of $x_{\mathrm{O_2,ox}}$ and $U_f$.

The global performance of the SOFC–mGT cycle is summarized in Fig 6 by plotting the normalized net electrical efficiency against the dry $CO_2$ mole fraction in the flue gas. Each point is color-coded by oxidant composition $x_{\mathrm{O_2,ox}}$ and classified according to the turbomachinery feasibility constraints. The feasible operating points, highlighted in circles (TIT$<$ 1000 °C and TOT$>$ 580 °C), form a distinct Pareto front representing the optimal trade-off between carbon capture potential and electrical efficiency. Each point collection represents one value of $U_f$, with the highest normalized efficiency representing $U_f = 0.3$ and the lowest $U_f = 0.8$.

A general inverse correlation between efficiency and $CO_2$ concentration emerges, reflecting the combined impact of thermodynamic and flow-field changes under oxygen enrichment. As $x_{\mathrm{O_2,ox}}$ increases, the combustor experiences higher adiabatic flame temperatures and reduced mass flow, leading to increased turbine inlet temperatures. Nevertheless, this efficiency penalty remains moderate across most of the examined range.

The Pareto-optimal region is populated predominantly by intermediate/high $U_f$ ($\approx$ 0.4–0.8), which consistently deliver dry $CO_2$ mole fractions above 18 % while sustaining normalized efficiencies up to 1.1 relative to the SOFC standalone efficiency. These conditions represent an effective compromise between combustion temperature, expansion work, and recuperation effectiveness. Within this range, the thermal and mass-flow balances of the turbomachinery remain favorable, keeping both TIT and TOT within safe operational limits while enhancing the $CO_2$ capture readiness of the cycle.

In contrast, infeasible operating points (shown as $\times$) cluster at the boundaries of the design space. At low $U_f$ ($< 0.4$), TIT surpasses material limits, as there is more fuel available for the combustor, producing thermal overloads near the turbine inlet. Conversely, at high/intermediate levels ($U_f > 0.5$), the greater presence of inert gas and lower adiabatic temperatures lead to TOT values below 580 °C, impeding effective recuperation and SOFC cathode preheating. Both conditions compromise system viability and thus lie outside the feasible design envelope.

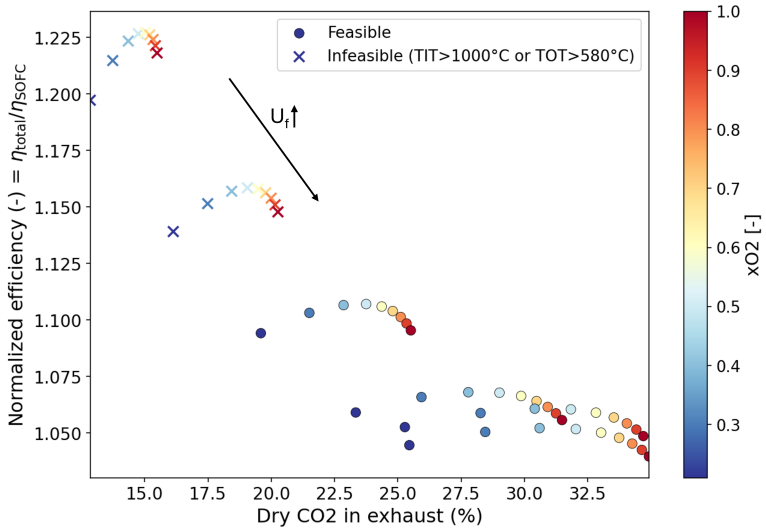


**Figure 6**: Normalized net electrical efficiency ($\eta_{\text{total}}/\eta_{\text{SOFC}}$) versus dry $CO_2$ mole fraction in the exhaust, with each point colour-coded by oxidant $O_2$ fraction $x_{O_2,\text{ox}}$. Points are classified by turbomachinery feasibility: circles (TIT$<1000$°C *and* TOT$>580$°C) vs. cross (infeasible). The Pareto front confirms that moderate enrichment ($x_{O_2,\text{ox}} \approx 0.5$) achieves the best compromise between $CO_2$ enrichment ($>22\%$) and high efficiency ($>1.1$) within feasible limits for $U_f = 0.5$.

Interestingly, the region of elevated $NO_x$ formation identified in Fig 3 overlaps with the infeasible high-TIT zone, demonstrating that emission control and thermal constraints can be decoupled through appropriate parameter tuning, especially at high $x_{O_2,\text{ox}}$. Specifically, maintaining $x_{O_2,\text{ox}}$ as high as possible mitigates the $NO_x$ penalty while preserving acceptable TIT and TOT values. At the opposite extreme, full oxy-combustion ($x_{O_2,\text{ox}} = 1.0$) yields the highest flue-gas $CO_2$ concentrations (exceeding 30 %), but the associated thermal and mass-flow penalties result in diminishing efficiency gains and tighter operational margins.

Overall, this analysis reveals a clear guideline for system optimization: combining moderate oxygen enrichment ($x_{O_2,\text{ox}} \approx 0.4$–$0.6$) with high SOFC fuel utilization ($U_f > 0.7$) enables simultaneous attainment of higher efficiency, robust $CO_2$ enrichment, and feasible turbomachinery operation. This finding reinforces the viability of partial oxy-combustion as a practical strategy for carbon capture integration in hybrid SOFC–microturbine systems.

It should be noted that the net efficiencies reported here do not account for the oxygen production penalty associated with the oxidant supply. When separation costs are considered, whether via cryogenic ASU, oxygen transport membranes, or electrolytic routes, the net efficiency advantage of partial oxy-combustion will narrow relative to the air-fired baseline, and the optimal enrichment level identified in Fig 6 may change.

# 5. Conclusion

This work investigated the combined effect of oxidant composition and SOFC fuel utilization on flue-gas $CO_2$ fraction, thermal-$NO_x$ formation potential, and cycle performance in an atmospheric SOFC–mGT hybrid system, with the aim of identifying operating windows where oxy-combustion yields a net benefit for carbon capture without compromising thermomechanical feasibility.

The results confirm that oxy-combustion is an effective lever for producing capture-ready exhaust streams in SOFC–mGT hybrids without requiring fundamental cycle redesign. $CO_2$ enrichment arises from two concurrently suppressible dilution mechanisms—electrochemical conversion of carbon-bearing fuel and elimination of $N_2$ from the oxidant stream—whose combined effect is sufficient to satisfy the feed thresholds of established capture technologies even under partial oxygen enrichment. Thermal-$NO_x$ formation is not monotonically suppressed across the air-to-oxy transition. A risk window of elevated formation potential persists at intermediate enrichment levels where elevated flame temperatures and residual $N_2$ availability reinforce one another, underscoring that enrichment

protocols must be designed with explicit awareness of this non-monotonic behavior to avoid transient emissions excursions.

The Pareto analysis reveals that partial oxy-combustion, rather than full oxy-firing, represents the more practically attractive near-term strategy: moderate enrichment combined with high fuel utilization simultaneously achieves acceptable $CO_2$ concentrations, favorable turbine temperatures, and competitive cycle efficiency. Full oxy-combustion delivers the highest capture readiness but at the cost of tighter operational margins and diminishing efficiency returns.

A key limitation of the present study is the omission of explicit oxygen production penalties. When separation costs are accounted for (via cryogenic ASU ($\sim$0.2–0.3 kWh/Nm$^3$ $O_2$), membrane separation, or electrolytic routes) the net efficiency advantage of partial oxy-combustion will narrow, and the optimal enrichment level may shift. Quantifying these penalties, alongside fuel-composition sensitivity and dynamic operability analysis, constitutes the primary direction for future work.

# Acknowledgments

This Research was funded by the CETPartnership Joint Call 2023 (Grant Agreement No. 2410153/2450340).

# Nomenclature

**Letter symbols**

| | |
|---|---|
| $\dot{m}_f$ | fuel mass flow rate, $\mathrm{kg/s}$ |
| $p$ | pressure, $\mathrm{Pa}$ |
| $T$ | temperature, $\mathrm{K}$ |
| $U_f$ | fuel utilization factor |
| $\dot{W}$ | power, $\mathrm{W}$ |
| $x$ | mole fraction |

**Greek symbols**

| | |
|---|---|
| $\eta$ | efficiency |

**Subscripts and superscripts**

| | |
|---|---|
| *comb* | combustor |
| *el* | electrical |
| *net* | net |
| *ox* | oxidant |

**Abbreviations**

| | |
|---|---|
| *ASU* | Air Separation Unit |
| *LHV* | Lower Heating Value |
| *mGT* | micro Gas Turbine |
| *SOFC* | Solid Oxide Fuel Cell |
| *TIT* | Turbine Inlet Temperature |
| *TOT* | Turbine Outlet Temperature |
| *VPSA* | Vacuum Pressure Swing Adsorption |

# References

[1] Leeper JD. *The gas turbine/fuel cell hybrid cycle*. In: Proceedings of the International Gas Turbine and Aeroengine Congress and Exhibition; 1999.

[2] Massardo AF., Lubelli F. *Internal reforming solid oxide fuel cell-gas turbine combined cycles (IRSOFC-GT): Part A–Cell model and cycle thermodynamic analysis*. J Eng Gas Turbines Power 2000;122(1):27–35.

[3] Damo UM., Ferrari ML., Turan A., Massardo AF. *Solid oxide fuel cell hybrid system: A detailed review of an environmentally clean and efficient source of energy*. Energy 2019;168:235–246.

[4] Azizi MA., Brouwer J. *Progress in solid oxide fuel cell-gas turbine hybrid power systems: System design and operating conditions optimization*. J Power Sources 2018;270:195–215.

[5] McLarty D., Brouwer J., Samuelsen S. *Fuel cell-gas turbine hybrid system design part I: Steady state performance*. J Power Sources 2014;257:412–420.

[6] Khalili-Garakani A., Mehrpooya M., Vatani A. *Propose and investigate a novel integrated process for the recovery of natural gas liquids and flare gas*. Process Saf Environ Prot 2021;107:540–553.

[7] Al-Khori K., Bicer Y., Koç M. *Integration of solid oxide fuel cells into oil and gas operations: Needs, opportunities, and challenges*. J Clean Prod 2021;riddled:125879.

[8] Oryshchyn D., Harun NF., Tucker D., Bryden KM., Shadle L. *Fuel utilization effects on system efficiency in solid oxide fuel cell gas turbine hybrid systems*. Appl Energy 2018;228:1953–1965.

[9] Rahimpour MR., Jokar SM. *Feasibility of flare gas reformation to practical energy in Farashband gas refinery: No gas flaring*. J Hazard Mater 2012;209–210:204–217.

[10] Wang Y., Banerjee A., Deutschmann O. *Dynamic analysis and control of a solid oxide fuel cell system for* $\mathrm{CO_2}$ *capture and utilization*. Energy Convers Manage 2023;277:116621.

[11] Bolland O., Undrum H. *A novel methodology for comparing* $CO_2$ *capture options for natural gas-fired combined cycle plants*. Adv Environ Res 2003;7(4):901–911.

[12] Zeldovich YB. *The oxidation of nitrogen in combustion and explosions*. Acta Physicochim URSS 1946;21:577–628.

[13] Lefebvre AH., Ballal DR. *Gas Turbine Combustion: Alternative Fuels and Emissions*. 3rd ed. Boca Raton, FL: CRC Press; 2010.

[14] Elcogen AS. *Elcogen SOFC Stack ES-Series Product Datasheet*. Available at: `https://elcogen.com` [accessed 2024].

[15] Gaitanis A., Vouros S., Zanios I., Kalfas AI. *Experimental assessment of a 10 kWe micro gas turbine under various operating conditions*. In: Proceedings of ASME Turbo Expo 2025; 2025.

[16] Vieira MCDJ., De Paepe W. *Steady-state analysis of an SOFC–mGT hybrid cycle with flare-gas surrogates*. Energy Proceedings 2026. )

[17] Smith GP., Golden DM., Frenklach M., Moriarty NW., Eiteneer B., Goldenberg M., et al. *GRI-Mech 3.0*. Available at: `http://combustion.berkeley.edu/gri-mech/` [accessed 2025].

[18] Goodwin DG., Speth RL., Moffat HK., Weber BW. *Cantera: An object-oriented software toolkit for chemical kinetics, thermodynamics, and transport processes*. Version 3.0. 2023. `https://www.cantera.org`. 10.5281/zenodo.8137090

[19] Aspen Technology Inc. *Aspen Plus User Guide: RGibbs Reactor Model*. Burlington, MA: Aspen Technology; 2023.

[20] Buhre BJP., Elliott LK., Sheng CD., Gupta RP., Wall TF. *Oxy-fuel combustion technology for coal-fired power generation*. Prog Energy Combust Sci 2005;31(4):283–307.

[21] Talebi-Anaraki A., Kaviri AG., Jaafar MNM., Pourpasha H., Amidpour M. *A review of the*

*$CO_2$ capture in power plants*. J CO2 Util 2023;68:102345.

[22] Biermann M., Ali H., Sundqvist M., Anheden M., Normann F., Harvey S. *Comparison of absorption-based post-combustion $CO_2$ capture with MEA at different $CO_2$ concentrations*. Int J Greenh Gas Con 2022;115:103614.

[23] Campanari S., Chiesa P., Manzolini G., Bedogni S. *Economic analysis of $CO_2$ capture from natural gas combined cycles using molten carbonate fuel cells*. Appl Energy 2016;185:125–137.

[24] Shen C., Liu Z., Li P., Yu J. *Two-stage VPSA process for $CO_2$ capture from flue gas using activated carbon beads*. Ind Eng Chem Res 2012;51(13):5011–5021.

[25] Cinti G., Bidini G., Hemmes K. *Comparison of the solid oxide fuel cell system for power and hydrogen production*. Front Energy Res 2022;10:1017829.